ELSEVIER

Sensors and Actuators A 97–98 (2002) 776–783

SENSORS AND ACTUATORS A PHYSICAL

www.elsevier.com/locate/sna

High amplification compliant microtransmissions for rectilinear electrothermal actuators

Larry L. Chu[a,*], Joel A. Hetrick[b], Yogesh B. Gianchandani[a,b]

[a]Department of Electrical and Computer Engineering, University of Wisconsin, Madison, WI 53706, USA
[b]Department of Mechanical Engineering, University of Wisconsin, Madison, WI 53706, USA

Accepted 21 November 2001

Abstract

This paper reports on synthesized designs of beam-based compliant microstructures used to modify the force–displacement relationships of electrothermal actuators. The design process uses a two-stage approach: truss elements are used for the topology synthesis and beam elements are used for the dimensional optimization. In order to accommodate buckling constraints, it limits the stress and the length of the beam segments. Measurements of devices fabricated from 11.5 μm thick p^{++} Si and 55 μm thick electroplated Ni as structural materials match theoretical predictions within 20%. Rectilinear non-resonant displacements up to 100 μm and displacement amplification factors >20× are obtained. The large displacement amplitude has a number of potential applications, including the switching or manipulation of optical fibers.
© 2002 Elsevier Science B.V. All rights reserved.

Keywords: Rectilinear bent-beam electrothermal actuators; Compliant mechanism; Microtransmission; Displacement amplification

1. Introduction

Electrothermal actuators are attractive for applications that benefit from high output forces, low actuation voltages, and electrically conductive structural materials. Simple and cascaded bent-beam electrothermal actuators have been used for rectilinear motion parallel to the substrate plane [1,2], producing maximum displacements and maximum blocking forces (defined as the forces which null the displacement) in the range of 8 μm and 2.5 mN, respectively, for a silicon device of 1000 μm length, 6 μm width, 4.5 μm thickness, and 0.2 rad bending angle, operating at 400 °C. However, in many applications a higher displacement is necessary, a smaller force is adequate (Fig. 1), and the operating speed of incremental mechanisms like inchworms is insufficient. This paper describes scalable, beam-based compliant microtransmissions that can be coupled to thermal actuators as shown in Fig. 2, to increase the peak displacement of electrothermal actuators from several microns to 100 μm.

Compliant mechanisms are structures that deform elastically to transmit a force or displacement [3–6]. Electrothermal actuation of compliant microstructures has been used in a variety of ways [1,2,7–9]. They are relatively immune to backlash and friction, and their monolithic designs are suitable for lithography-based fabrication. These aspects make them attractive for microsystem applications.

Past applications of microtransmissions to rectilinear actuators have included the use of electrostatic actuators. In [10], an electrostatic actuator offering displacements up to 20 μm was reported. In contrast, this paper explores compliant mechanism topologies as microtransmissions for electrothermal devices, which provide much higher force. The challenge in designing a high performance compliant mechanism is to optimize the structural topology, size and geometry to efficiently transform the forces of an input actuation source to drive an output load. While the synthesis of compliant mechanisms [4–6] and combined electrothermal complaint actuators [7,8] has been reported in the past, the approach developed here using truss and beam elements can precisely control the force–displacement trade-off at extreme levels of amplitude magnification.[1] The topologies that have been developed to provide geometric advantages of 3–21×, resulting in static displacements up to ≈100 μm. The use of stress constraints in the design permits this performance to be achieved with relatively thin structural material and low aspect ratio (<2 in most cases). Devices are fabricated using both heavily boron doped single crystalline

* Corresponding author. Tel.: +1-608-263-3982.
E-mail addresses: chul@cae.wisc.edu (L.L. Chu), hetrick@flxsys.com (J.A. Hetrick), yogesh@umich.edu (Y.B. Gianchandani).

[1] Portions of this paper have appeared in conference abstract in [11,12].

0924-4247/02/$ – see front matter © 2002 Elsevier Science B.V. All rights reserved.
PII: S0924-4247(02)00020-1

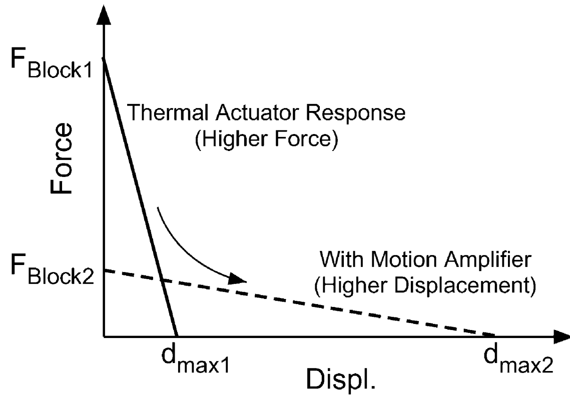

Fig. 1. A compliant micro-transmission provides rectilinear motion and allows the force–displacement trade-off to be tailored for an application.

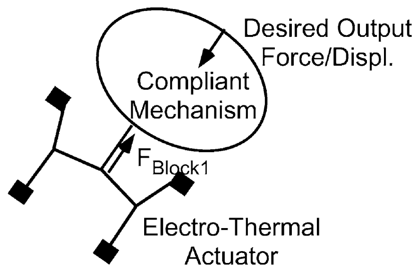

Fig. 2. The topology design problem for a compliant mechanism rectilinear amplifier.

(p^{++}) Si and electroplated Ni as structural materials. The design procedure and test results are presented in the following sections.

2. Design synthesis

The design procedure is broken into topology synthesis and dimensional synthesis. Each stage is posed as a structural optimization problem, where the objective is to maximize the blocking force and/or unloaded output displacement given all relevant design constraints. The primary characteristics of the actuator are the block force, F_{block1} (i.e. the maximum force at zero displacement) and unloaded output displacement, d_{out1}. When a compliant mechanism is coupled to an electrothermal actuator, it can transform these two quantities to produce a new block force, F_{block2}, and unloaded output displacement, d_{out2}. Depending on the design, the compliant mechanism can achieve extreme amplification of the block force or output displacement, as required by the application. The amplification magnification factor, A, is expressed as the ratio of the output displacement to the input (actuator) displacement:

$$A = \frac{d_{\mathrm{out2}}}{d_{\mathrm{out1}}} \quad (1)$$

While amplification change is one method for evaluating the performance, other methods such as specifying the ratio of blocking forces can also be readily accommodated. For example, the factor M is defined as a function of slope change between the input and output force–displacement characteristics:

$$M = \sqrt{\frac{d_{\mathrm{max2}} F_{\mathrm{block1}}}{d_{\mathrm{max1}} F_{\mathrm{block2}}}} \quad (2)$$

Analysis is performed using structural truss and beam elements along with linear, static finite element theory (for the moment coupled electrical and thermal effects are neglected). For both topology synthesis and dimensional synthesis, the finite element equilibrium analysis and the constrained optimization problem are solved within MATLAB™. Optimization is performed using MATLAB's sequential quadratic programming (SQP) algorithm. Design derivatives are calculated using the adjoint variable method and by directly differentiating the stiffness matrix with respect to size and node position design variables.

The generic structural optimization problem (for both topology and dimensional synthesis) is posed as follows:

$$\mathrm{Max}\left\{ F_{\mathrm{block2}} d_{\mathrm{out2}} - P\left(\frac{d_{\mathrm{out2}}}{d_{\mathrm{out1}}} - A^*\right)^2 \right\} \quad (3)$$

subject to:

$$\sigma_{\mathrm{axial}} - \sigma_{\mathrm{buckling}} \leq 0, \quad V - V_{\mathrm{allow}} \leq 0, \quad h_{\mathrm{min}} \leq h_i \leq h_{\mathrm{max}},$$
$$X_{\mathrm{min}} \leq X_j \leq X_{\mathrm{max}}, \quad Y_{\mathrm{min}} \leq Y_k \leq Y_{\mathrm{max}}$$

The required amplification factor, A^*, is enforced by penalizing the objective function by the penalty factor, P, which is empirically chosen. It tends to impact the topology synthesis more than the dimensional synthesis. Different iterations using varying values of P were performed. The design that was selected offered the highest output displacement and blocking force in addition to satisfying the amplification factor. Buckling is enforced by limiting the maximum axial stress to $\sigma_{\mathrm{buckling}}$ based on Euler's buckling criteria, modified for end conditions (during dimensional synthesis). The total volume constraint is enforced by V_{allow}. Design variables include element width and node position co-ordinates denoted by h_i, X_j, and Y_k, respectively. During dimensional synthesis, these are given local upper and lower bounds that serve to limit the search space and also enforce fabrication limitations.

To establish the optimal topology of a mechanism, the design domain is discretized using a network of truss elements, defined as a ground structure. The topology optimization process seeks to resize each element width until the performance of the structure is maximized. Upon completion, elements that converge to the lower bound are removed yielding the final mechanism topology. The topology synthesis approach described here utilizes a modular ground structure where nodes are allowed to change location within 'wandering limits'. Research has shown that this technique produces good topology designs that accurately satisfy magnification requirements [13].

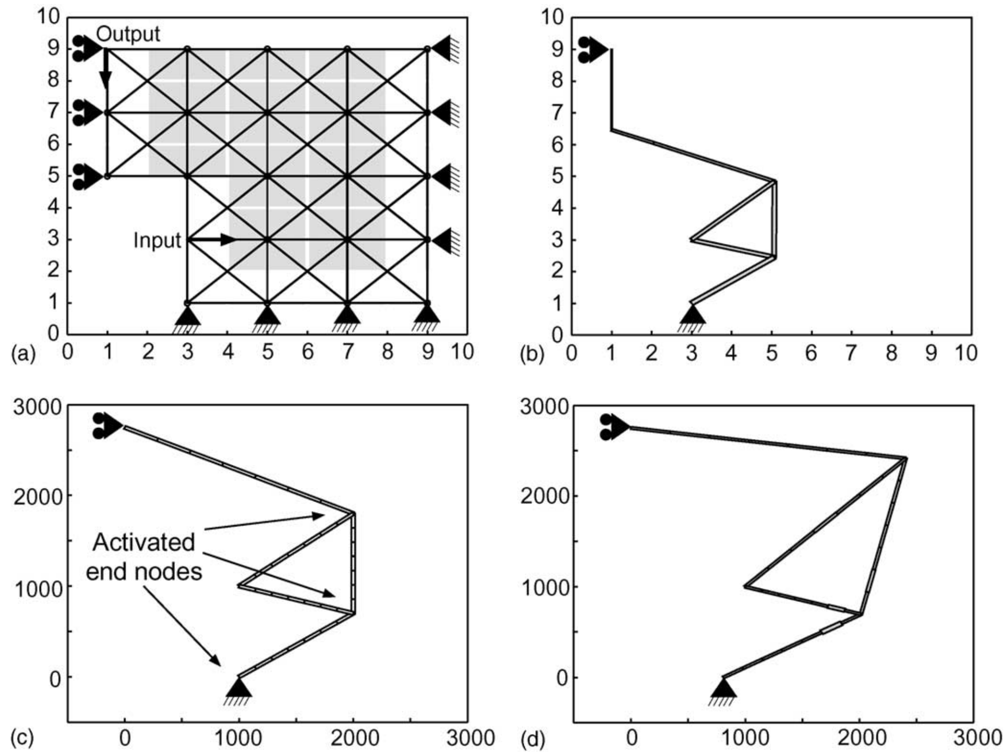

Fig. 3. Steps in the synthesis of the two-input microtransmission, showing half of the complete structure. (a) Assuming symmetry, half the design domain is meshed with truss elements; (b) optimized topology is determined; (c) design is re-meshed for dimensional synthesis; (d) final design obtained. The moving boundary conditions on the *y*-axis have only one degree of freedom due to symmetry.

Since the actuators are symmetrical about the axis of motion, the microtransmissions can take advantage of symmetry, which allows only half of the topology to be designed, which lowers computational requirements. For the following example, the modulus was set to 1000, the width was set to 1, the total volume constraint was set to 2, and the lower element bound was set at 1×10^{-4}. To achieve the amplitude magnification factor of 20, the penalty multiplier was set to 1. Fig. 3a shows the floating-node ground structure, discretized using 25 nodes and 72 elements; 23 nodes were activated and given wandering ranges resulting in 107 design variables (wandering ranges indicated by gray areas). Fig. 3b indicates the optimal topology of the compliant mechanism amplifier with elements converging to the lower bound removed.

To proceed with dimensional synthesis, each segment of the topology is re-meshed using arrays of beam elements; the number of elements along an array is directly controlled by the designer. Exact specifications for the material modulus, out-of-plane thickness, input actuator characteristics, and desired magnification are input into the optimization routine. The designer may choose to activate end nodes of topology segments, allowing for geometric variation. Intermediate nodes along the length of an activated segment are adjusted by maintaining a collinear equidistant relationship.

Fig. 3c shows the example from the topology synthesis re-meshed for the secondary dimensional synthesis stage. Constraints within the fabrication sequence that pose upper or lower bonds on the various dimensions of the structural components can be defined at this point. In this example, the thickness and the minimum widths of the elements were set to 15 μm. Fig. 3d shows the optimized structure ($A^* = 20, P = 1, V_{\text{allow}} = 1 \times 10^6\ \mu\text{m}^3$). This particular design offers a blocking force of 470 μN assuming a Young's modulus (E) of 100 GPa, and a free displacement of 51 μm. The force is proportional to E. Because of the minimum width limitation, substantial energy is spent deforming the compliant transmission (transmission efficiency is 14.1%). Larger blocking force and free displacement can be achieved by fabricating more flexible structures with thinner beam widths (within buckling limitations). Fig. 4 shows the steps in the synthesis of another design for which a single in-line input is required.

The final design of the two-input single output amplifier of Fig. 3 is shown in Fig. 5. The entire web-like mechanism is suspended above the substrate and attached to it only at the anchors (i.e. the cross-hatched portions). Current is passed between the nodes V^+ and V^-. The symmetry of the design confines the current to centrally located bent-beam actuators, which provide lateral input displacements to the microtransmission. This generates an axial displacement at the output node, as shown. Incorporation of stress constraints in Eq. (3) to reduce the propensity for out-of-plane buckling results in the selective widening of beams that are in compression when actuated. The final version of the single input amplifier of Fig. 4 is shown in Fig. 6. In both the single

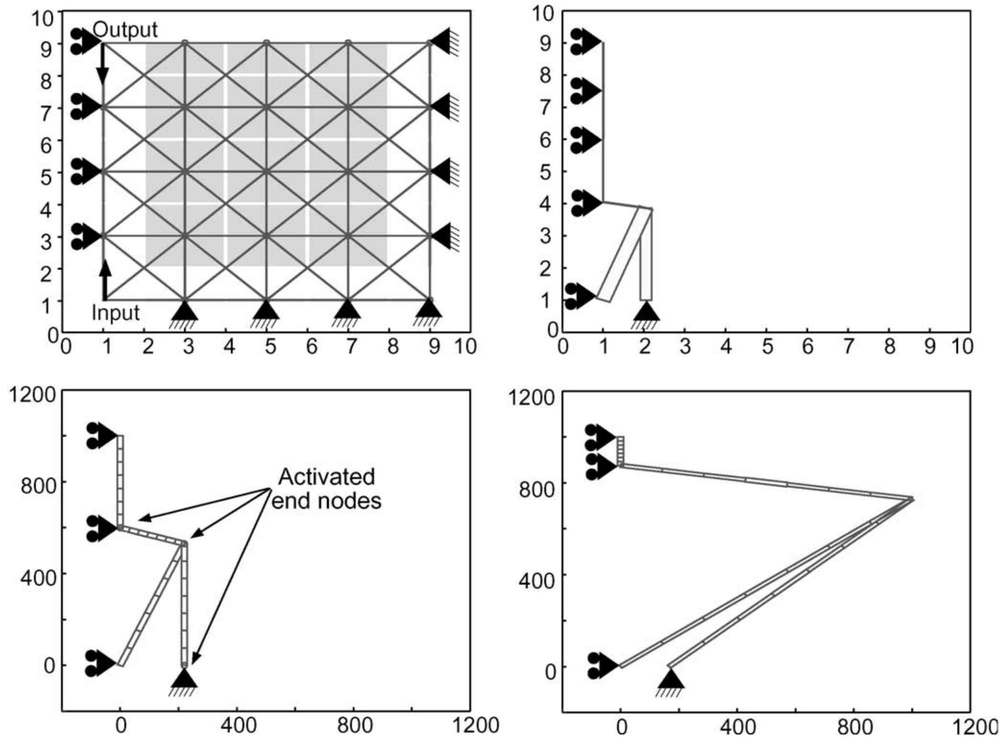

Fig. 4. Steps in the synthesis of the single input microtransmission. The moving boundary conditions have the same constraints as in Fig. 3.

input and two-input devices, the greatest amplification is provided by the shallow bent-beam at the output, which is in tension.

Fig. 7 shows results from the finite element analysis (FEA) of a device of the type shown in Fig. 5. Since the device is laterally symmetric, only half the structure was modeled. The dimensional variables were as noted for device LA in Table 1. Material properties reflected the use of p^{++} Si (boron-doped ⟨1 0 0⟩ single crystal) as the structural material. The thickness of the entire structure was assumed to be 11.5 μm. This shows the load line of an individual bent-beam actuator, along with a family of load lines at the output of the mechanism under different levels of actuation. The level of actuation, which is controlled by the electrical power applied to the bent-beams, is represented by the parameter F_{block1}. It is clear from this that the microtransmission converts a load line which has force and displacement axis intercepts of 6 mN and 5.8 μm, to those which have intercepts in the range of 250 μN and 100 μm,

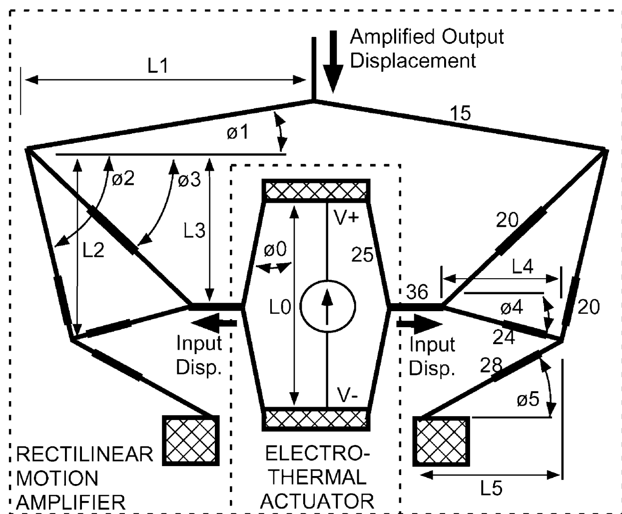

Fig. 5. A synthesized microtransmission with two bent beam actuators providing lateral input forces. Cross-hatched areas represent anchors which attach structure to substrate.

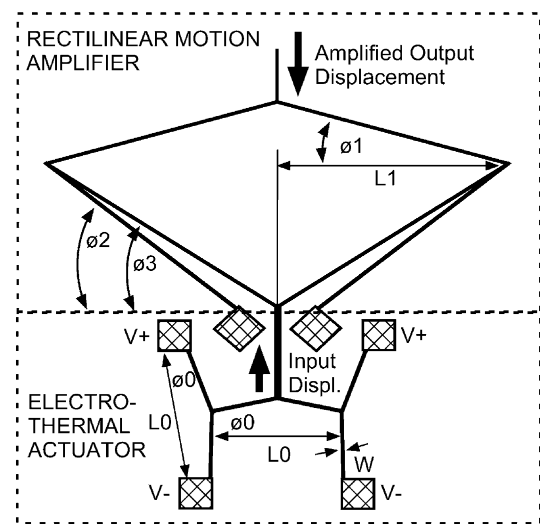

Fig. 6. Schematic of the single input rectilinear microtransmission and cascaded actuator showing the dimensional variables.

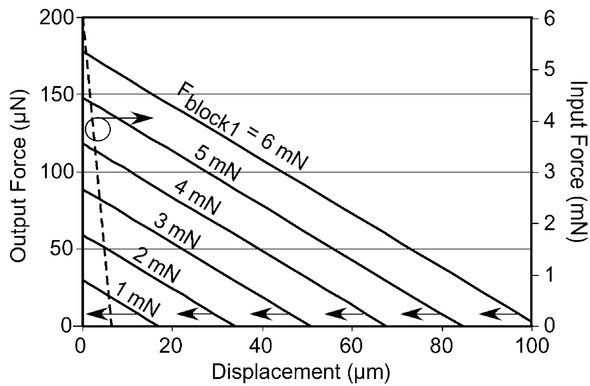

Fig. 7. Load lines for an individual bent-beam actuators and for a symmetric half of device LA with the topology of Fig. 2 and dimensions as defined in Table 1.

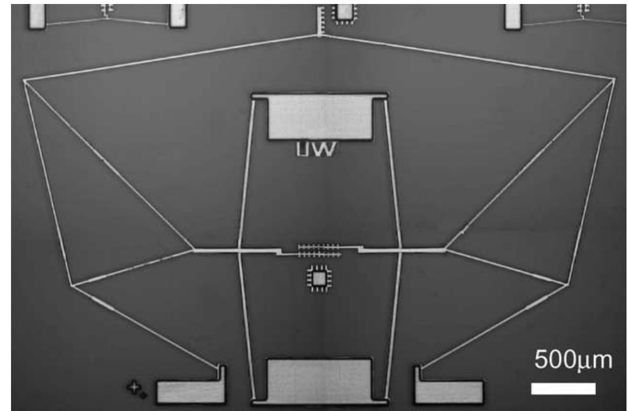

Fig. 8. A p^{++} Si implementation of device LA.

respectively. It is important to note that the FEA was performed for only half the structure, and the actual output force is twice that indicated in Fig. 7. The calculated amplification factor, A_{calc}, is 17.5 for this device.

From a design perspective, it is convenient to begin with the target force and displacement required at the output of the mechanism. If A and M are known for the selected transmission, the force and displacement required at its input can be calculated. The bent-beam actuator can then be designed using the analytical equations for its unloaded displacement (d_{out1}) and maximum force (F_{block1}) described in [1]. It must be able to provide the force and displacement required by the transmission without buckling.

3. Fabrication

Microtransmissions with electrothermal actuators were demonstrated using electroplated Ni structures by surface micromachining and the LIGA process, and using single crystal p^{++} Si by the dissolved wafer process.

To implement the dissolved wafer process [14], field area of the silicon wafer is first recessed by 3 μm to form the anchors. A blanket boron diffusion for 12 h in a diffusion furnace using solid sources results in an 11.5 μm deep p^{++} Si junction. The structures were defined by a 14 μm-deep RIE step using SF_6, which cuts through the diffused layer. The silicon wafer is then anodic bonded to a (#7740) glass substrate. Finally, the devices were released in an EDP-based silicon etchant, leaving the 11.5 μm thick p^{++} Si structures. An optical micrograph of a typical device, device LA, is shown in Fig. 8.

Surface micromachined Ni devices were fabricated on silicon wafers insulated with 1 μm thick thermal oxide and 0.5 μm thick LPCVD nitride. A 2 μm thick sputtered Ti sacrificial layer was patterned and covered with a Cr/Ni seed layer. The devices were electroplated into a photoresist mold from a nickel sulfamate solution. At 55 °C temperature, the plating current was adjusted to provide a structural layer thickness of 16 μm in 120 min. Devices with other thickness were also electroplated at the same rate. The photoresist mold was subsequently stripped and the sacrificial material etched away. Some samples were then covered with a thin layer of gold by electrode-less plating to provide an inert coating. Optical images of fabricated structures are shown in Fig. 9.

Another set of devices was fabricated on (#7740) glass substrates (Fig. 10) using LIGA technology [15]. These devices were plated on a 2 μm thick Cu sacrificial layer using a Ni sulfamate solution which had Ni concentration of 82 g/l. At 56 °C temperature and 32 mA/cm^2 current density, a thickness of 55 μm was achieved in 95 min. The LIGA devices benefit from precise dimensional control and better sidewalls profile. For the electroplating conditions

Table 1
Dimensions of fabricated devices as defined in Figs. 5 and 6. R_w denotes ratio of actual beam widths to those indicated

Device #	L0 (μm)	L1 (μm)	L2 (μm)	L3 (μm)	L4 (μm)	L5 (μm)	R_w	Thickness	Material	Technology	Topology
LA	2450	2415	1750	1400	1000	1210	1.0	11.5	p^{++} Si	Bulk	Two input
LB	2450	2180	1450	1150	985	1105	1.0	11.5	p^{++} Si	Bulk	Two input
LC	1838	1182	1313	1050	750	908	0.71	11.5	p^{++} Si	Bulk	Two input
S1	1225	1208	875	700	500	605	0.42	11.5	p^{++} Si	Bulk	Two input
LIGA	980	1090	720	580	495	570		55	Ni	LIGA	Two input
A	1000	1000	Not applicable for single input mechanisms					10.8	Ni	Surface	Single input
D	720	1500						70	Ni	Surface	Single input
B	1000	1200	840	690	500	580		10.5	Ni	Surface	Two input
C	1000	1080	720	570	490	550		10.5	Ni	Surface	Two input

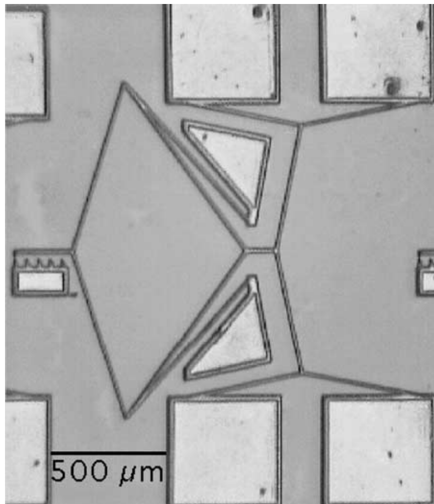

Fig. 9. Optical micrographs of device A, a cascaded bent-beam actuator with attached microtransmission. The devices were fabricated from Ni electroplated on Si substrates.

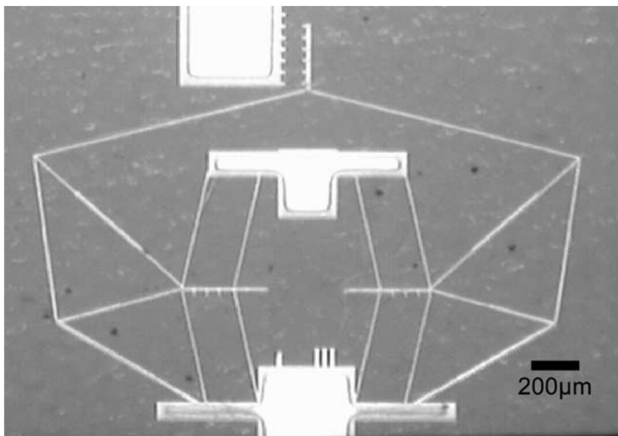

Fig. 10. Device LIGA, an implementation of microtransmission with electrothermal actuators using 55 μm thick Ni as structural material.

used, the Young's modulus was measured to be 115 ± 10 GPa [16].

4. Experimental results

The fabrication processes yielded a number of microtransmissions located at the ends of electrothermal actuators. During testing, a current was passed through the electrothermal actuators and the displacements were measured at both the input and output of the microtransmission. The measurements were taken by a calibrated visual method, with an uncertainty of <0.5 μm. The dimensional parameters of designs that were fabricated are defined in Figs. 5 and 6 and tabulated in Table 1.

In the LIGA device, the microtransmission was driven by two pairs of bent-beam actuators at each lateral input

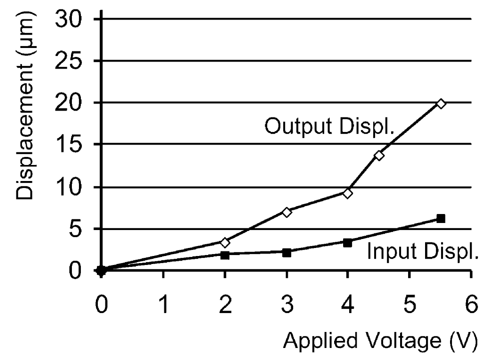

Fig. 11. Measured input and output displacement responses for device D under electrothermal actuation.

(Fig. 10). A displacement of 85 μm was measured at a current of 900 mA and nearly 0.9 W of power. The displacement amplification factor was measured to be 9.3, as compared to the calculated value of 8.2. The resistance of the 55 μm Ni device was <850 mΩ. Although the driving voltage was consequently <0.9 V, the amount of current required for this device is too high for many applications. In addition, parasitic contact resistances of a few hundred milliohms can waste substantial power. For thick structures, a material with higher resistivity such as p^{++} Si, can provide a better compromise of moderate current and voltage.

Surface micromachined Ni devices A (Fig. 9) and D implement the one-input and one-output design topology in which the input of the mechanism is driven by a cascaded bent-beam actuator. Device B and C has a topology similar to the LIGA device, with two input ports. Device D had a measured amplification of 3.1 and was electrothermally actuated to 19.5 μm (Fig. 11). Device A was tested by mechanical actuation, not electrical actuation, in order to examine the behavior of the mechanism near the proximity of buckling. (The actuator was not able to generate enough displacement in this particular design to reach the out-of-plane buckling threshold; this was observed during device testing.) The device exhibited an amplification of 12.9 and generated up to 80 μm of output displacement before any significant out-of-plane deformation was observed (Fig. 12). Once buckling occurs, the amplification performance degrades severely. This finding underscores the importance to synthesis mechanisms that are optimized to resist buckling. Device C was also actuated mechanically and achieved a maximum displacement of 145 μm without out-of-plane buckling (with an amplification factor of 11.0). Device B was actuated with applied current and reached 30 μm at an input power of 364 mW (Fig. 13).

Even though Ni has a relatively high thermal expansion coefficient of about 13.5 ppm/K [16], which is highly desirable in making a thermal actuator, it has certain limitations: (1) the electro-deposited Ni has a relatively low Young's modulus of 115 GPa; (2) the maximum operation temperature in air is relatively low (∼350 °C); and (3) the electrical resistivity is too low for thick structures. In order to maximize

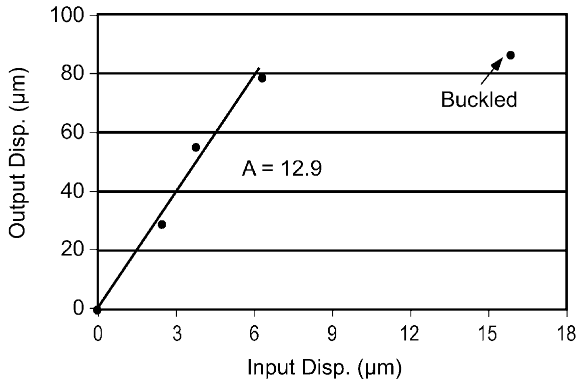

Fig. 12. Measured ratio of input to output displacement for the microtransmission of device E (Table 1). This measurement was taken mechanically because of operating temperature limitations.

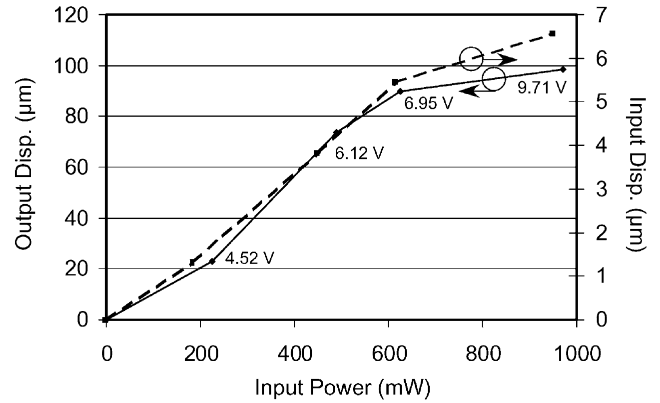

Fig. 14. Measured displacement at the input (d_{out1}) and output (d_{out2}) of the microtransmission for device LA.

the output force, a high Young's modulus is desirable. Even though the Young's modulus of bulk Ni is 208 GPa, it was found that electro-deposited Ni has a much lower modulus [14]. Operation temperature is the peak temperature that is reached in an actuator when it is heated. Ni structures start to degrade at about 350 °C, and catastrophic failure occurs at below 500 °C. Although the exact mechanism is not clear, it is believed that oxidation and temperature induced resistance lowering are likely to be among the causes. Finally, the high conductivity of Ni translates into high current requirements as noted previously. In contrast, p^{++} Si has a higher Young's modulus (~180 GPa), lower electrical conductivity, and a higher maximum operation temperature (~700 °C); all these attributes make p^{++} Si an appealing choice.

The p^{++} Si device LA is shown in Fig. 8; it achieved 100.4 μm output displacement when driven by 105 mA and <10 V, and the measured amplification factor was 17.0. This compares very well with the predicted value of 17.5. The detailed response of this device is shown in Fig. 14. Its best use appears to be at output displacements below 90 μm for which the input power is about 650 mW. Device LB reached 34 μm output displacement with an amplification of 8.6 (Fig. 15). Device LC achieved 86.2 μm output displacement when driven by 85 mA current (Fig. 16). Its displacement amplification factor of 21.4 was higher than predicted, possibly because a portion of the suspension may have been heated. Additional results can be found in Table 2, along with calculated performance. As predicted, p^{++} Si structures outperformed their Ni counterparts.

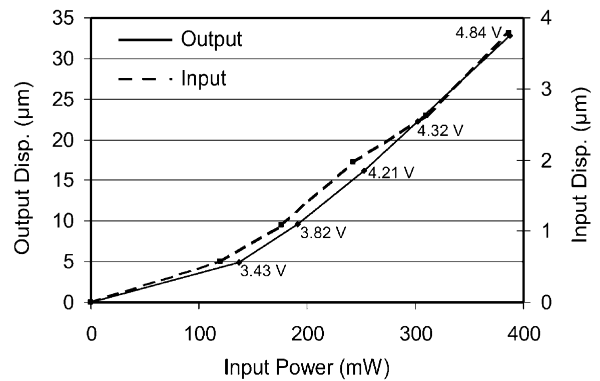

Fig. 15. Measured displacement at the input (d_{out1}) and output (d_{out2}) of the microtransmission for device LB.

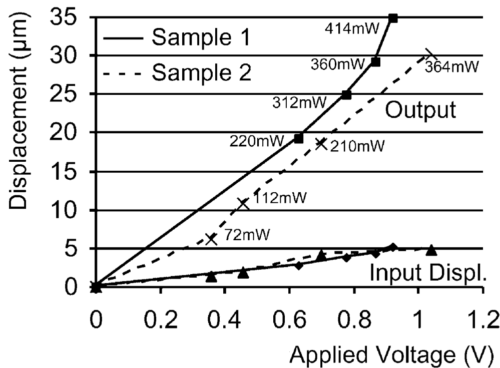

Fig. 13. Measured input and output displacement response for two device B structures.

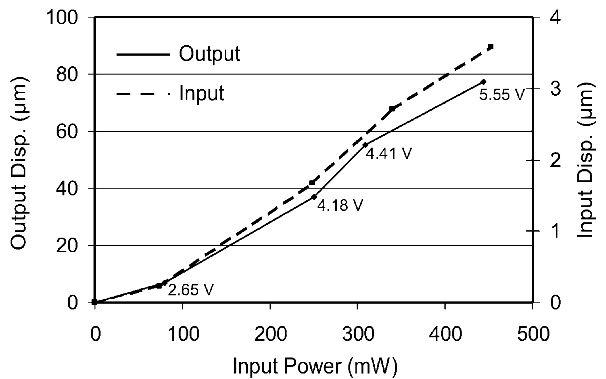

Fig. 16. Measured displacement at the input (d_{out1}) and output (d_{out2}) of the microtransmission for device LC.

Table 2
Summary of simulated and measured results[a]

Device #	I (mA)	Measured		Estimated	
		A_{meas}	d_{out2} (μm)	A_{calc}	F_{block2} (μN)
LA	105	17.0	100.4	17.5	174.5
LB	90	8.6	34.1	9.1	306.6
LC	86.2	21.4	85.0	17.5	–
S1	47.6	18.6	55.0	17.6	66.4
LIGA	~900	9.3	85	8.2	–
A	Mech[b]	12.9	>80	14.1	>235
D	–	3.1	19.5	3.2	–
B	364	13.5	31.0	19.5	–
C	Mech[b]	11.0	145	9.5	–

[a] For p^{++} Si structural material, assume uniform $\Delta T = 500$ °C, 3 ppm/K expansion coefficient, and $E = 180$ GPa. For Ni structures, assume uniform $\Delta T =< 500$ °C, ~13.5 ppm/K expansion coefficient, and $E = 115$ GPa.
[b] Device was actuated mechanically to observe buckling behavior.

5. Conclusions

Microtransmissions have been used to tailor the force–displacement relationships of electrothermal actuators. Topology synthesis and dimensional synthesis are demonstrated to effectively automate the design of compliant mechanisms obtaining high magnification values. The two-stage process produces detailed designs given the actuator and material input parameters while considering magnification, out-of-plane buckling, and minimum width constraints.

Two topologies were generated by the synthesis algorithm; one with a single input and the other with two inputs. Both topologies have only one output node. Several designs were achieved with these topologies, with varying amplification and mechanical characteristics. To demonstrate the flexibility of the synthesis algorithm, these designs have amplifications span from 3 to 21×.

The compliant microtransmissions with electrothermal actuators were fabricated using electroplated Ni and p^{++} Si. It was demonstrated that the mechanism performs well for all of the technologies tested. The measured amplification factors for all the devices tested agree well with in 20% with the design values, which demonstrated up to 21× displacement amplification. The majority of the mechanisms tested achieved >50 μm non-resonant output displacement, and a maximum displacement of ~100 μm was reached by two of the devices tested. Mechanisms with displacement amplitude in this order can be applied to optical fiber manipulation.

References

[1] L. Que, J.-S. Park, Y.B. Gianchandani, Bent-beam electrothermal actuators—Part I: single beam and cascaded devices, J. Microelectromech. Syst. 10 (2) (2001) 247–254.

[2] J.S. Park, L.L. Chu, A.D. Oliver, Y.B. Gianchandani, Bent-beam electrothermal actuators—Part II: linear and rotary microengines, J. Microelectromech. Syst. 10 (2) (2001) 255–262.

[3] S. Kota, J. Hetrick, Z. Li, L. Saggere, Tailoring unconventional actuators using compliant transmissions: design methods and applications, IEEE/ASME Trans. Mech. 4 (4) (1999) 396–408.

[4] O. Sigmund, Tailoring materials with prescribed elastic properties, Mech. Mater. 20 (1995) 351–368.

[5] G. Ananthasuresh, S. Kota, N. Kikuchi, Strategies for systematic synthesis of compliant MEMS, in: Proceedings of the 1994 ASME Winter Annual Meeting on Dynamic Systems and Control, DSC-Vol. 55, No. 2, Chicago, IL, November 1994, pp. 677–686.

[6] S. Nishiwaki, M. Frecker, M. Seungjae, N. Kikuchi, Topology optimization of compliant mechanisms using the homogenization method, Int. J. Numer. Meth. Eng. 42 (3) (1998) 535–559.

[7] T. Moulton, G. Ananthasuresh, Micromechanical devices with embedded electro-thermal-compliant actuation, in: Proceedings of the ASME International Mechanical Engineering Conference and Exposition, MEMS, MEMS-Vol. 1, Nashville, TN, November 1999, pp. 553–560.

[8] J. Jonsmann, O. Sigmund, S. Bouwstra, Compliant thermal microactuators, Sens. Actuat. 76 (1999) 463–469.

[9] H. Guckel, J. Klein, T. Christenson, K. Skrobis, M. Laudon, E. Lovell, Thermo-magnetic metal flexure actuators, in: Proceedings of the Solid-state Sensor and Actuator Workshop, Hilton Head, SC, June 1992, pp. 73–75.

[10] S. Kota, J. Hetrick, Z. Li, S. Rodgers, T. Krygowski, Synthesizing High-performance Compliant Stroke Amplification Systems for MEMS, in: Proceedings of the IEEE International Conference on MEMS, Miyazaki, Japan, January 2000.

[11] L. Chu, J. Hetrick, Y. Gianchandani, Electro-thermal actuators using optimized compliant microtransmissions as rectilinear motion amplifiers, in: Proceedings of the Solid-state Sensors Actuators Workshop, Hilton Head, SC, June 2000.

[12] L. Chu, J. Hetrick, Y. Gianchandani, Compliant microtransmissions for rectilinear electrothermal actuators, in: Proceedings of the Transducers, Munich, Germany, 2001, pp. 714–717.

[13] J. Hetrick, A unified approach for topological and dimensional synthesis of compliant mechanisms, Ph.D. Thesis, University of Michigan, Ann Arbor, MI, 1999.

[14] Y. Gianchandani, K. Najafi, A bulk silicon dissolved wafer process for microelectromechanical systems, IEEE J. Microelectromech. Syst. 1 (2) (1992) 77–85.

[15] H. Guckel, High-aspect-ratio micromachining via deep X-ray lithography, Proc. IEEE 86 (8) (1998) 1586–1593.

[16] L. Chu, L. Que, Y. Gianchandani, Temperature coefficients of material properties for electrodeposited MEMS, in: Proceedings of the IEEE International Conference on MEMS, Interlaken, Switzerland, January 2001.